
Verify when Uncertain: Beyond Self-Consistency in Black Box Hallucination Detection

Yihao Xue^{1,2} Kristjan Greenewald³ Youssef Mroueh⁴ Baharan Mirzasoleiman¹

Abstract

Large Language Models (LLMs) suffer from hallucination problems, which hinder their reliability in sensitive applications. In the black-box setting, several self-consistency-based techniques have been proposed for hallucination detection. We empirically study these techniques and show that they achieve performance close to that of a supervised (still black-box) oracle, suggesting little room for improvement within this paradigm. To address this limitation, we explore cross-model consistency checking between the target model and an additional verifier LLM. With this extra information, we observe improved oracle performance compared to purely self-consistency-based methods. We then propose a budget-friendly, two-stage detection algorithm that calls the verifier model only for a subset of cases. It dynamically switches between self-consistency and cross-consistency based on an uncertainty interval of the self-consistency classifier. We provide a geometric interpretation of consistency-based hallucination detection methods through the lens of kernel mean embeddings, offering deeper theoretical insights. Extensive experiments show that this approach maintains high detection performance while significantly reducing computational cost.

1. Introduction

Large Language Models (LLMs) have extremely powerful abilities to answer questions or summarize or explain content. However, hallucinations have emerged as a persistent problem, where plausible-looking but incorrect information is mixed in with the generations. Hallucinations create major difficulties for both human users and tool calling or agentic applications due to their visual plausibility, as verifying all portions of the model generation is often just as hard as finding the answer using legacy methods.

A key challenge is detecting hallucinations in black-box scenarios, where we can access only an LLM’s outputs but not its intermediate states—an especially relevant concern when using closed-source commercial APIs. An important intuition is that *self-consistency*—mutual entailment between multiple stochastically sampled high-temperature generations from the LLM for the same question—is lower when the model is hallucinating compared to when it provides a correct answer. As Tolstoy wrote in *Anna Karenina*, “All happy families are alike; every unhappy family is unhappy in its own way.” Mechanistically, this LLM behavior can be understood as follows, from the fact that LLMs are pretrained as *statistical* language models. If the model confidently knows the answer, then probability should be concentrated on that answer. If, on the other hand, the model does not know all or part of the answer, its statistical pretraining will bias it towards creating what is essentially a posterior distribution on answers or parts of answers that seem plausible.

Following this philosophy, prior work (Manakul et al., 2023; Farquhar et al., 2024; Kuhn et al., 2023; Lin et al., 2023; Nikitin et al., 2024) has proposed various methods that leverage self-consistency. However, it remains unclear how much further they can be improved. Thus, we investigate whether we are already near the performance ceiling, given the limited information available in a black-box setting. Using a unified formalization of self-consistency-based methods, we design a method that trains graph neural networks to approximate the ceiling performance of this method family. Notably, we find that existing methods are already close to this ceiling, suggesting little room for further improvement within this paradigm.

This highlights the need to go beyond self-consistency alone. Thus, we consider the case where an additional model serves

¹Department of Computer Science, University of California, Los Angeles ²Work performed while interning at MIT-IBM Watson AI Lab ³MIT-IBM Watson AI Lab ⁴IBM Research. Correspondence to: Yihao Xue <yihaoxue@g.ucla.edu>.

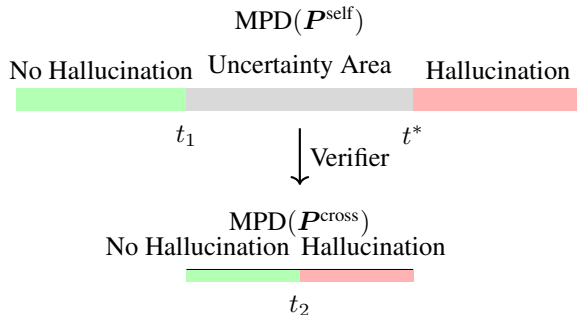


Figure 1: Two Stage Hallucination Detection. First, the self-consistency matrix P^{self} is formed and the test statistic is computed. This is thresholded with two thresholds, where medium values (gray region) advance to the second stage for disambiguation. The P^{cross} cross-consistency matrix and test statistic are then computed for these ambiguous samples for final classification.

as a verifier, and we incorporate consistency checking between answers generated by the target model and the verifier. This approach provides information that self-consistency alone cannot capture. For example, agreement between the two models increases confidence in a response’s correctness, while disagreement suggests that at least one model is likely hallucinating. Through experiments, we observe a significant gain in the approximated ceiling performance when both self-consistency and cross-model consistency are taken into account, interestingly, even when the verifier is weaker than the target model. Additionally, we find that linearly combining self-consistency with cross-model consistency can achieve performance very close to this ceiling.

Finally, we address the computational overhead introduced by the verifier model. We propose a budget-aware method that performs cross-model consistency checking for only a specified fraction of questions, keeping the computation budget controllable. This method consists of two stages (illustrated in Fig. 1): first, it performs self-consistency checking; then, it selectively applies cross-model consistency checking only when self-consistency falls in a middle range, where judgment is less reliable. We provide a geometric interpretation of this approach through the lens of kernel mean embeddings, offering theoretical insights into its effectiveness. Through extensive experiments across three datasets and 20 target-verifier combinations, we demonstrate that this adaptive mechanism can achieve high detection performance while significantly reducing computational costs. Additionally, we provide practical suggestions on selecting verifier models based on different budget constraints.

2. Related Work

There are works that explore white-box detection methods, such as (Duan et al., 2024; Varshney et al., 2023), which require token-level logits, or (Yin et al., 2024; Zou et al., 2023; Agrawal et al., 2023), which rely on intermediate representations. White-box methods are less suitable for certain scenarios, such as closed-source commercial APIs. In this work, we focus exclusively on black-box hallucination detection, where we do not have access to the internal workings of the LLM. In this scenario, the primary approach involves checking the consistency between multiple samples of the LLM’s answers (Manakul et al., 2023; Farquhar et al., 2024; Kuhn et al., 2023; Lin et al., 2023; Nikitin et al., 2024). These works rely on sampling multiple answers to the same question from the LLM and using an NLI (Natural Language Inference) model to determine whether they are semantically equivalent. The NLI judgments are then processed in various ways to decide whether a hallucination has occurred. Details of these methods are discussed in Section 4. Manakul et al. (2023); Kuhn et al. (2023) also explore alternative methods for judging semantic equivalence, which are either less effective (e.g., n-gram) or computationally expensive (e.g., using an LLM). (Zhang et al., 2023) identify limitations in self-consistency-based methods and propose leveraging question perturbation and cross-model response consistency (comparing an LLM’s responses with those from an additional verifier LLM) to improve performance. While their approach improves results, introducing a verifier model adds computational overhead. In this work, we systematically explore the possibility of achieving computational efficiency when combining self-consistency and cross-model consistency. Note that the question perturbation technique from (Zhang et al., 2023) is orthogonal to our approach and could potentially be incorporated to achieve better results. Another line of work involves directly asking LLMs to judge the uncertainty of their answers (Mielke et al., 2022; Tian et al., 2023b; Kadavath et al., 2022; Lin et al., 2022), which typically requires additional finetuning/calibration and does not fit within the black-box scenario. Without any modification to the original LLMs, their verbalized confidence is often inaccurate (Xiong et al., 2023). The inherent conflict between calibration and hallucination, as theoretically

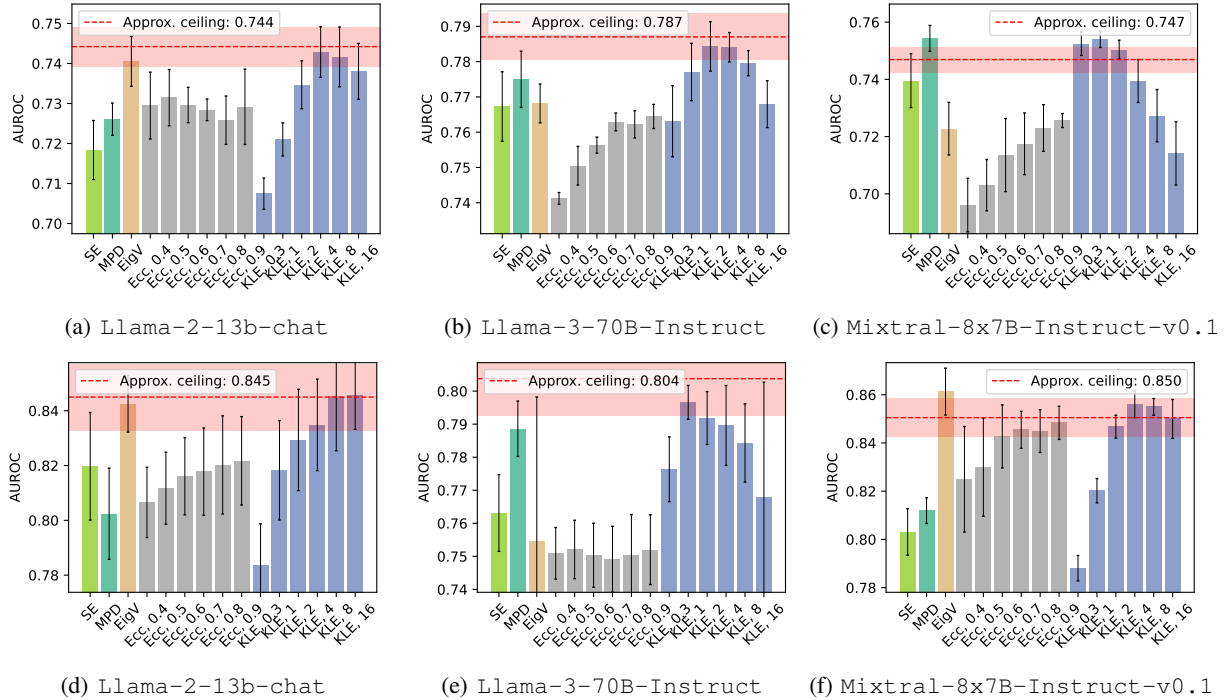


Figure 2: Comparison between AUROC of existing methods and the approximated ceiling performance on SQuAD ((a)–(c)) and TriviaQA ((d)–(f)). We observe that, across all setups, the best method performs very close to the oracle, indicating that we are approaching the performance limit. A similar result is observed for AURAC in Fig. 7.

shown in (Kalai & Vempala, 2024), further highlights the limitations of this approach. There are also works addressing hallucination mitigation, such as using RAG (Asai et al., 2023; Gao et al., 2022), inference-time intervention (Li et al., 2024), or fine-tuning (Lee et al., 2022; Tian et al., 2023a), which is beyond the scope of this paper.

3. Preliminaries

In the task of hallucination detection, we have a target LLM, denoted by \mathcal{M}_t , for which we aim to detect hallucinations. We are given a set of questions $\{q_i\}_{i=1}^n$. Given a set of questions $\{q_i\}_{i=1}^n$, the model generates answers, $a_i = \mathcal{M}_t(q_i, \tau)$, under a specified temperature τ . The ground truth annotation \hat{h}_i indicates whether a_i is a hallucination ($\hat{h}_i = 1$) or factual ($\hat{h}_i = 0$). The objective is to predict whether a_i is a hallucination, with our prediction denoted by h_i .

To achieve this, many methods are designed to output a value, v_i , that captures specific characteristics (e.g., the uncertainty of the answer). A higher value of v_i suggests that a_i is more likely to be a hallucination. The prediction h_i is then determined based on a threshold applied to v_i , where the choice of threshold dictates the final classification.

To evaluate the performance of a hallucination detection method, we focus on two widely accepted metrics computed given outputs $\{v_i\}_{i=1}^n$ and ground truths $\{\hat{h}_i\}_{i=1}^n$: (1) **AUROC**, area under the receiver operating characteristic curve. is a classic performance measure in binary classification. It captures the trade-off between the true positive rate and the false positive rate across various thresholds, providing an aggregate measure of the model’s ability to distinguish between the two classes. (2) **AURAC**, the area under the “rejection accuracy” curve (Farquhar et al., 2024). It is designed for scenarios where a hallucination detection method is employed to refuse answering questions that the model is most likely to hallucinate on. Rejection accuracy measures the model’s accuracy on the $X\%$ of questions with the lowest v_i values (least likely to hallucinate), and the area under this curve summarizes performance across all values of X .

4. From Self-consistency to Cross-Consistency

4.1. Self-consistency based detection

Prior work (Manakul et al., 2023; Farquhar et al., 2024; Kuhn et al., 2023; Lin et al., 2023; Nikitin et al., 2024) has introduced various methods leveraging self-consistency. However, the extent to which these methods can be further improved remains unclear. To explore this, we develop a method to approximate the ceiling performance for any approach that utilizes self-consistency and compare it against the performance of existing methods.

Unified formalization of self-consistency-based methods. We first present a unified formalization of the existing methods. Recall that the goal is to determine whether each $\mathcal{M}(q_i)$ is a hallucination. All these methods rely on additionally sampling m answers from the LLM \mathcal{M} for question q_i under a high temperature τ' , which is typically much higher than τ , the temperature used to generate a_i . For example, in (Farquhar et al., 2024), the settings are $\tau = 0.1$ and $\tau' = 1.0$. Let $\{a'_{i,j}\}_{j=1}^m$ denote the set of these additionally sampled answers. These methods then use an entailment estimator (e.g., DeBERTa-Large-MNLI), denoted by \mathcal{E} . The estimator \mathcal{E} takes two answers as input and outputs a value between 0 and 1, indicating the degree of entailment between the two answers, where 1 means full entailment. Using \mathcal{E} , a self-entailment matrix $\mathbf{P}_i^{\text{self}}$ is constructed as: $\mathbf{P}_i^{\text{self}} = [\mathcal{E}(a'_{i,j}, a'_{i,k})]_{1 \leq j \leq m, 1 \leq k \leq m}$, where each element is the entailment value for a pair of answers in $\{a'_{i,j}\}_{j=1}^m$. Existing methods can then be formalized as some function f applied to the self-entailment matrix $\mathbf{P}_i^{\text{self}}$ which outputs a scalar. The focus of prior work lies in designing various forms of f . Specifically, (1) $\text{SE}(\mathbf{P}_i^{\text{self}})$, the Semantic Entropy (Farquhar et al., 2024), uses a binarized version of $\mathbf{P}_i^{\text{self}}$ to identify which answers belong to the same semantic set and then computes the entropy over these semantic sets. (2) $\text{MPD}(\mathbf{P}_i^{\text{self}})$ (Lin et al., 2023; Manakul et al., 2023) is simply the mean pairwise distance, computed as $1 - \text{Mean}(\mathbf{P}_i^{\text{self}})$. (3) $\text{EigV}(\mathbf{P}_i^{\text{self}})$ (Lin et al., 2023) is defined as the sum of the eigenvalues of the graph Laplacian of $\mathbf{P}_i^{\text{self}}$. (4) $\text{Ecc}(\mathbf{P}_i^{\text{self}})$ (Lin et al., 2023) measures the eccentricity of the answers leveraging the eigenvectors of the graph Laplacian of $\mathbf{P}_i^{\text{self}}$. (5) $\text{KLE}(\mathbf{P}_i^{\text{self}})$, the Kernel Language Entropy (Nikitin et al., 2024), involves applying the von Neumann entropy to a graph kernel derived from $\mathbf{P}_i^{\text{self}}$. For all these methods, a higher output indicates greater uncertainty among $\{a'_{i,j}\}_{j=1}^m$, making the corresponding low-temperature answer a_i more likely to be a hallucination.

The underlying assumption is that $\mathbf{P}_i^{\text{self}}$ contains exploitable information related to \hat{h}_i , the ground truth hallucination annotation. This prompts the question: how much information does $\mathbf{P}_i^{\text{self}}$ actually encode about \hat{h}_i ? To explore this, we aim to identify the optimal function f that maps $\mathbf{P}_i^{\text{self}}$ to the hallucination label. This leads to the following formulation:

$$\hat{f} = \arg \min_f \mathbb{E}[l(f(\mathbf{P}_i^{\text{self}}), \hat{h})], \quad (1)$$

where l is a loss function that measures the discrepancy between the output value and the actual label.

Approximating the ceiling performance with GCN models. To search for \hat{f} , we frame it as a learning problem. Since the task is ultimately binary classification based on the matrix $\mathbf{P}_i^{\text{self}}$, graph neural networks are well-suited due to their ability to process matrix structures and express a wide range of functions. We use a two-layer Graph Convolutional Network (GCN) to represent f . The model is trained with BCE loss on sampled pairs of $\mathbf{P}_i^{\text{self}}$ and \hat{h} . We then evaluate AUROC and AURAC of the resulting model as an approximation of the ceiling performance. The training and test samples are drawn independently to account for the finiteness of the data, ensuring that the evaluation reflects the model’s ability of capturing a generalizable relationship between $\mathbf{P}_i^{\text{self}}$ and \hat{h} , rather than that of overfitting the training data.

Results. In Figs. 2 and 7, we compare the performance of existing methods with the ceiling performance approximated using the aforementioned approach across various settings. We consider three different LLMs: Llama-2-13b-chat, Llama-3-70B-Instruct, and Mixtral-8x7B-Instruct-v0.1, as well as two datasets: SQuAD and TriviaQA. In the plots, the x-axis represents different methods with varying hyperparameters. The best-performing method varies across different settings, with MPD, KLE, and EigV consistently showing relatively strong performance. Notably, in each setting, the top method closely approaches the approximated ceiling, indicating that existing methods already make near-maximal use of $\mathbf{P}_i^{\text{self}}$, particularly when sufficient validation data is available to optimize method and hyperparameter selection.

4.2. Incorporating cross-model consistency

As noted in the previous subsection, existing methods bring us very close to the ceiling performance for self-consistency alone. The question now is: how can we push beyond this limit? In the black-box scenario, our options are constrained by the lack of access to any internal model information. (Zhang et al., 2023) has explored another potential approach: leveraging outputs from other LLMs to improve hallucination detection through cross-model comparisons. A minimal

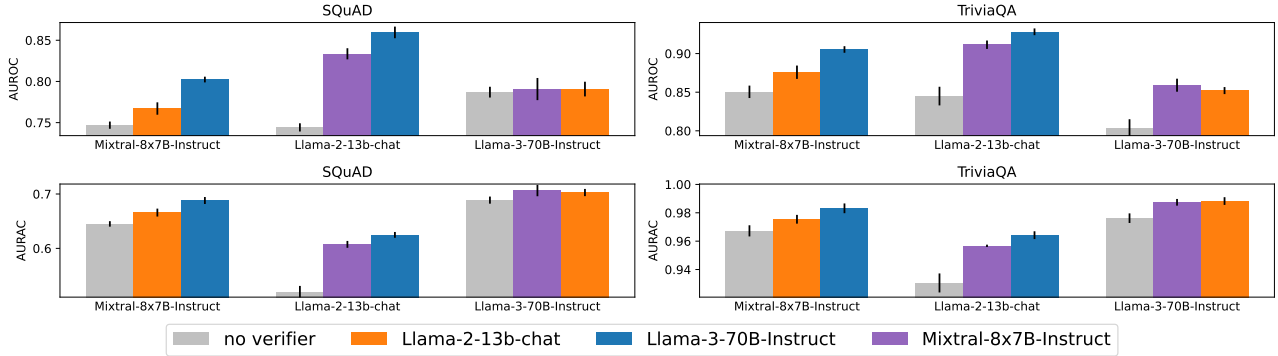


Figure 3: Comparison between approximated ceiling performances using only P^{self} (gray) and those using both P^{self} and P^{cross} . The x-axis shows the target model, and the colors indicate the verifier model, as shown in the legend. We observe a clear improvement when a verifier model is used, in terms of both AUROC and AURAC.

case involves using one additional model as a verifier. This added layer of information can help further refine hallucination detection. For example, if two models significantly disagree on their answers, at least one is likely hallucinating.

4.2.1. IMPROVEMENT IN THE CEILING PERFORMANCE

We explore how much gain cross-model consistency checking can possibly bring. Let us denote this verifier model as \mathcal{M}_v . Similar to the self-consistency case, a natural extension is to encode the cross-model consistency information in a matrix: $P_i^{\text{cross}} = [\mathcal{E}(a_{i,j}^t, b_{i,k}^v)]_{1 \leq j \leq m, 1 \leq k \leq m}$, where $\{b_{i,k}^v\}_{k=1}^m$ are m answers sampled from \mathcal{M}_v under temperature τ' for question q_i . Thus, P_i^{cross} captures the pairwise entailment relationships between the answers generated by the target model \mathcal{M}_t and the verifier model \mathcal{M}_v .

Remark 4.1 (Cross entailment). To build intuition, consider the setting of a very strong verifier model that always returns a sample from the ground truth distribution. Then, if the entailment model returns a calibrated posterior probability of entailment, it is easy to see that $\text{Mean}(P_i^{\text{cross}})$ is the probability of entailment between an \mathcal{M}_t sample and a ground truth sample. In other words, it can be interpreted as the probability of correctness. For as the verifier becomes weaker, we hypothesize that the $\text{Mean}(P_i^{\text{cross}})$ retains significant correlation with the probability of correctness, and observe this in practice.

Building on the formalization in Section 4.1, we aim to determine how much information can be extracted when both P^{self} and P^{cross} are used to predict the ground truth hallucination label. To achieve this, we search for a function f that takes both P^{self} and P^{cross} as input. Given the pairwise nature of the data, we again leverage GCN models to represent the function. Specifically, we combine P^{self} and P^{cross} into a single matrix: $\begin{bmatrix} P^{\text{self}} & P^{\text{cross}} \\ P^{\text{cross}} & \mathbf{0} \end{bmatrix}$ which encodes the underlying structure of the data as pairwise relationships between answers. We then apply a GCN to this combined matrix and train the model to fit the ground truth labels \hat{h} . Finally, we evaluate the resulting model to approximate the ceiling performance achievable with both P^{self} and P^{cross} .

We now compare the approximated ceiling performances achieved using only P^{self} to those achieved using both P^{self} and P^{cross} , as shown in Fig. 3. The x-axis represents the target model, while the colors indicate the verifier model used. Gray bars correspond to the scenario where only P^{self} is used, i.e., no verifier model is involved. The results demonstrate a clear improvement in performance, measured by both AUROC and AURAC, when a verifier model is introduced. Interestingly, this improvement is observed even in cases where the target model itself is quite strong. For example, on the TriviaQA dataset, adding a weaker verifier model can still enhance detection performance when Llama-3-70B-Instruct is used as the target model. This highlights the potential of leveraging cross-model consistency, as even a less powerful verifier can provide complementary insights that enhance hallucination detection.

4.2.2. LINEARLY COMBINING MDPs CLOSELY APPROACHES THE CEILING

Although the function the GCN implements to achieve ceiling performance is unknown, interestingly, we find that a simple extension of existing methods can perform almost equally well. We leverage MPD introduced earlier, which can be naturally extended to P^{cross} as $\text{MPD}(P^{\text{cross}}) = 1 - \text{Mean}(P^{\text{cross}})$. The combined approach uses a weighted average:

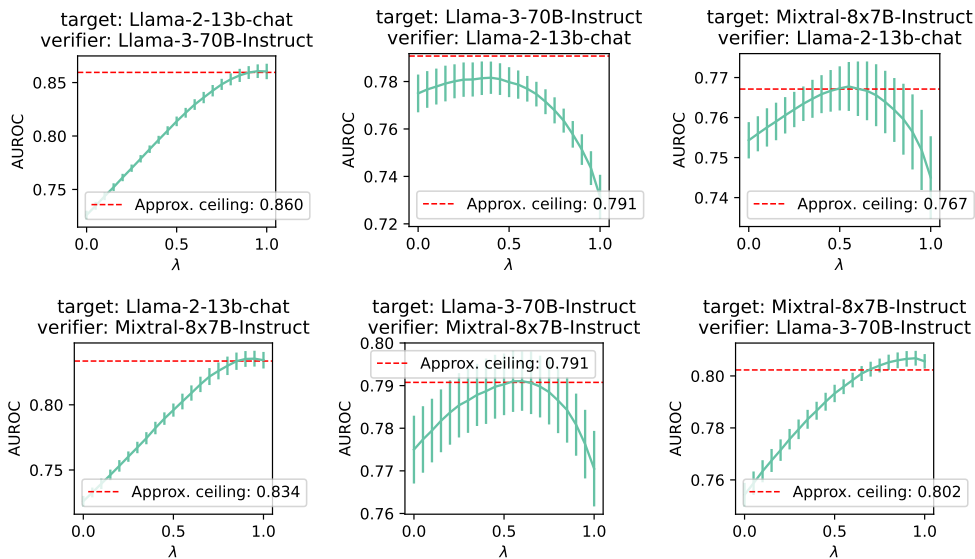


Figure 4: A simple weighted average of self-consistency and cross-consistency-based metrics, $(1 - \lambda)\text{MPD}(\mathbf{P}^{\text{self}}) + \lambda\text{MPD}(\mathbf{P}^{\text{cross}})$, can achieve performance close to that of the oracle method. Plots for AURAC are in Fig. 8 in Appx. C.2.

Algorithm 1 Budget-aware two-stage detection

Input: question q , target model \mathcal{M}_t , verifier model \mathcal{M}_v , number of samples m , temperature τ' , entailment estimator \mathcal{E} , thresholds t_1, t_2, t^* .
 $\{a'_j\}_{j=1}^m \leftarrow$ the m responses sampled from \mathcal{M}_t for the question q under temperature τ' {First stage}
 $\mathbf{P}^{\text{self}} \leftarrow [\mathcal{E}(a'_j, a'_k)]_{1 \leq j \leq m, 1 \leq k \leq m}$
 $s^{\text{self}} \leftarrow \text{MPD}(\mathbf{P}^{\text{self}})$
if $s^{\text{self}} < t_1$ **then**
 return $h = \text{false}$ {no hallucination}
else if $s^{\text{self}} > t^*$ **then**
 return $h = \text{true}$ {hallucination}
else
 $\{b'_j\}_{j=1}^m \leftarrow$ the m responses sampled from \mathcal{M}_v for the question q_i under temperature τ' {Second stage}
 $\mathbf{P}^{\text{cross}} \leftarrow [\mathcal{E}(a'_j, b'_k)]_{1 \leq j \leq m, 1 \leq k \leq m}$
 $s^{\text{cross}} \leftarrow \text{MPD}(\mathbf{P}^{\text{cross}})$
 return $h = \text{false}$ if $s_i^{\text{cross}} < t_2$ **else true**
end if

$(1 - \lambda)\text{MPD}(\mathbf{P}^{\text{self}}) + \lambda\text{MPD}(\mathbf{P}^{\text{cross}})$, where λ is a hyperparameter. As shown in Fig. 4, with an appropriate choice of λ , this method achieves performance very close to the approximated ceiling performance.

5. Budget-Aware Hallucination Detection with A Verifier Model

From the previous section, we observe that performance improves significantly when self-consistency checking is combined with cross-model consistency checking. However, this approach can introduce substantial computational overhead, especially when the verifier is a large model. For instance, with a 7B target model and a 70B verifier model, cross-model consistency adds 10 times the computation.

To address this issue, we propose a method to control computational overhead. As illustrated in Fig. 1. The key idea is to perform cross-model consistency checking only when it is most necessary. Intuitively, when self-consistency scores are extremely high or low, it is likely—though not guaranteed—that the model’s output is non-hallucinatory or hallucinatory, respectively. In such cases, performing cross-model consistency checking may not be necessary under limited computational budgets. Instead, cross-model consistency should focus on cases with intermediate self-consistency scores, where our judgment is more uncertain. This is formalized in Alg. 1. The parameter p specifies the fraction of instances for which cross-model consistency checking will be performed. The parameter t_1 is the threshold for $\text{MPD}(\mathbf{P}^{\text{self}})$ below which the

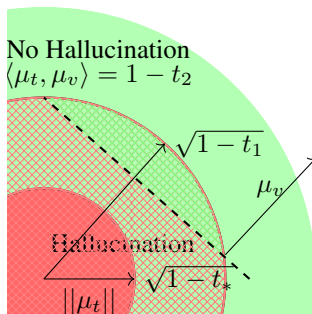


Figure 5: Geometric interpretation in mean embeddings spaces of “target” (μ_t) and “verifier” distributions (μ_v). Self consistency is measured via the norm of mean embeddings of the target model, and cross consistency via the dot product between mean embeddings. In stage one, detection is based on $\|\mu_t\|$, and we have no hallucination outside the sphere of radius $\sqrt{1-t_1}$ (in green) and hallucination within the sphere of radius $\sqrt{1-t_*}$ (in red). Between the two sphere the hyperplane defined by μ_v and t_2 , splits this area in two zones: above it for no hallucination (dashed green) and below it for hallucination (dashed red).

output is deemed non-hallucinatory. Based on t_1 , we choose to compute t^* , the threshold for $\text{MPD}(\mathbf{P}^{\text{self}})$ above which the output is classified as hallucinatory, such that only p of the $\text{MPD}(\mathbf{P}^{\text{self}})$ scores fall between t_1 and t^* . For these intermediate cases, judgments are made based on cross-model consistency $\text{MPD}(\mathbf{P}^{\text{cross}})$ using a threshold t_2 .¹ Note that we use MPD to measure inconsistency from \mathbf{P}^{self} due to its simplicity, ease of extension to $\mathbf{P}^{\text{cross}}$ (unlike, e.g., KLE, which is specifically designed for \mathbf{P}^{self} but not immediately well-defined for $\mathbf{P}^{\text{cross}}$), and the fact that it contains sufficient information for achieving ceiling performance, as discussed in Sec. 4.2.2. Future work could explore other metrics.

Geometric Interpretation in Mean Embedding Space. We provide a geometric interpretation of our hallucination detection. For each prompt x we can observe the conditional distribution of the target model $\pi_t(y|x)$ and the verifier $\pi_v(y|x)$. In particular we observe $\frac{1}{n_a} \sum_{i=1}^{n_a} \delta_{y_i^a}, y_i^a \sim \pi_t(\cdot|x)$ and $\frac{1}{n_v} \sum_{i=1}^{n_v} \delta_{y_i^v}, y_i^v \sim \pi_v(\cdot|x)$. We assume that the entailment kernel $\mathcal{E} : \mathcal{Y} \times \mathcal{Y} \rightarrow [0, 1]$ to be a reproducing kernel. The mean embeddings (Muandet et al., 2017) of target, verifier and ground truth are respectively $\mu_t = \frac{1}{n_a} \sum_{i=1}^{n_a} \mathcal{E}(y_i^a, \cdot)$, $\mu_v = \frac{1}{n_v} \sum_{i=1}^{n_v} \mathcal{E}(y_i^v, \cdot)$, and $\mu^* = \frac{1}{n^*} \sum_{i=1}^{n^*} \mathcal{E}(y_i^*, \cdot)$. We can write the self-consistency in terms of norms of mean embeddings :

$$\|\mu_t\|^2 = \frac{1}{n_a^2} \sum_{i,j} \mathcal{E}(y_i^a, y_j^a) = 1 - \text{MPD}(\mathbf{P}^{\text{self}})$$

and the cross-consistency

$$\langle \mu_t, \mu_v \rangle = \frac{1}{n_a n_v} \sum_{i,j} \mathcal{E}(y_i^a, y_j^v) = 1 - \text{MPD}(\mathbf{P}^{\text{cross}})$$

Fig. 5 gives a geometric interpretation of our two stage algorithm in means embedding spaces. If the “target” model norm of mean embedding is higher than a threshold $\sqrt{1-t_1}$ no hallucination is detected and for a norm less than a threshold $\sqrt{1-t^*}$ is detected. For the uncertainty area between the two spheres, the verifier mean embedding defines with the threshold $1-t_2$ a hyperplane that divides this area in no hallucination (above) and hallucination (below).

Evaluating AUROC/AURAC for Algorithm 1. Recall that, in the conventional scenario, the AUROC and AURAC metrics are defined for a system that outputs a single value for binary classification. To compute these metrics, we vary the threshold used to produce the label from the output. In such cases, for both ROC and RAC curves, each X -value corresponds to a single Y -value. For example, in ROC, one false positive rate corresponds to one true positive rate, allowing us to obtain a single curve by varying the threshold and then compute the area under it. However, the situation is more complex for our Algorithm 1, which, given a fixed hyperparameter p , ultimately outputs binary labels but involves two thresholds, t_1 and t_2 . Different combinations of t_1 and t_2 can yield the same X -value but different Y -values, resulting in a plot that resembles a thick band rather than a single curve. Thus, the area under the curve is not well-defined. The way these thresholds are adjusted relative to each other significantly affects the Y values for a given X . To derive a meaningful performance measure for our algorithm, we establish the relationship between the two thresholds using a validation set. Specifically, on this set,

¹We threshold $\text{MPD}(\mathbf{P}^{\text{cross}})$ directly in the second stage (instead of a linear combination as in Section 4.2.2, since (a) it saves a hyperparameter and (b) we are able to approach the GCN-based performance ceiling without it.

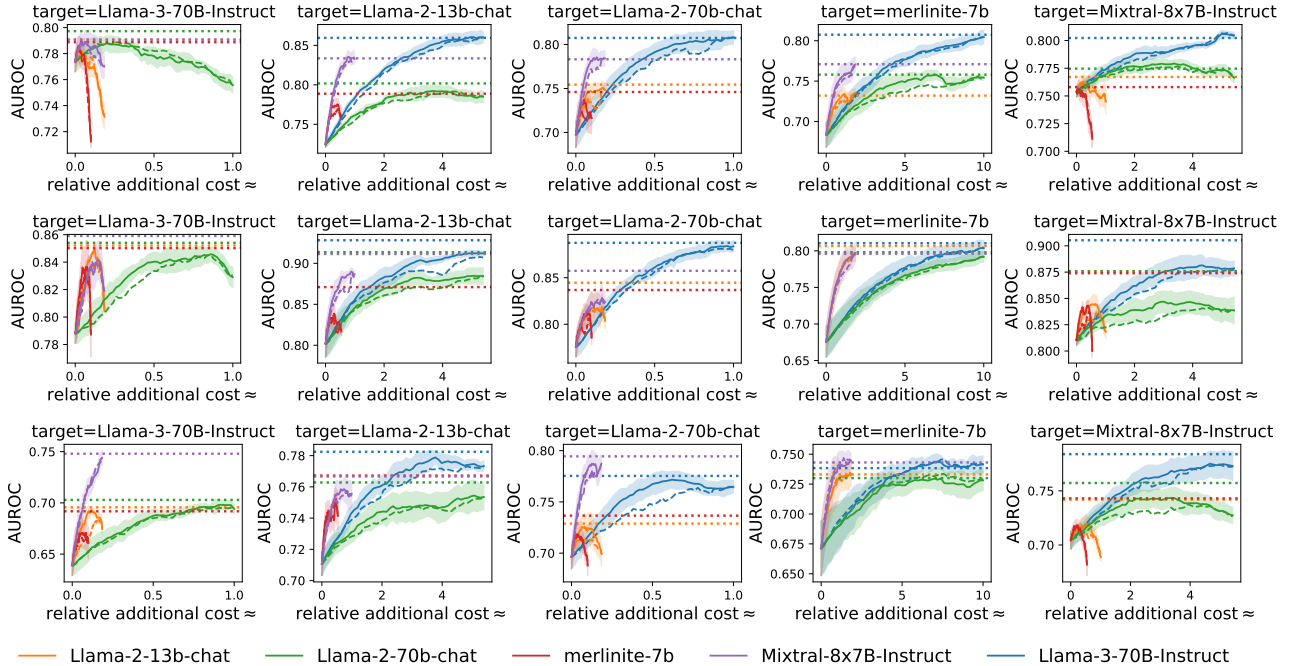


Figure 6: We plot AUROC against the *relative additional cost* for SQuAD (top), TriviaQA (middle), and Natural Questions (bottom). Solid curves represent results where the validation set consists of independent samples for the same questions, while dashed curves correspond to validation sets consisting of answers for different questions. The dotted horizontal line indicates the approximate ceiling performance using GNN. The curves are mostly convex, indicating that a small number of cross-model consistency checks contribute to most of the performance improvement. This demonstrates that our approach can achieve high performance with very low cost, which is further evidenced in Table 1. Results for AURAC are in Fig. 9.

we iterate over a grid of threshold combinations, running the algorithm to obtain all X, Y pairs. For each small interval of X , we identify the threshold combinations that maximize Y . Next, we use a separate test set, where we only evaluate the good combinations identified from the validation step and compute the resulting AUROC/AURAC. We note that prior work (Lin et al., 2023; Nikitin et al., 2024) also relies on a validation set for tuning hyperparameters.

We now prove that the above procedure for selecting the two thresholds from data achieves a test-time AUROC close to the optimal value achieved on the validation set. Our theorem below applies more generally to any method that uses data to select from a finite set of threshold values.

Theorem 5.1 (AUROC Generalization). *Suppose we are given n_{neg} i.i.d. samples from the non-hallucinating distribution and n_{pos} i.i.d. samples from the hallucinating distribution, and sets of candidate thresholds $\mathcal{T}_1 = \{t_j^1\}_{j=1}^{|\mathcal{T}_1|}$ and $\mathcal{T}_2 = \{t_k^2\}_{k=1}^{|\mathcal{T}_2|}$ for stages 1 and 2 respectively. Suppose we use this data to choose a mapping $t_1, t_2 = \mathcal{A}(p_{FA})$ from desired probability of false alarm level $p_{FA} \in [0, 1]$ to thresholds $t_1 \in \mathcal{T}_1, t_2 \in \mathcal{T}_2$, maximizing the probability of detection on the validation data. Let $A_{val}(\mathcal{A})$ be the AUROC using thresholds given by \mathcal{A} . Then, with probability at least $\left(1 - \frac{2}{|\mathcal{T}_1||\mathcal{T}_2|}\right)^2$, the test AUROC satisfies $A_{test}(\mathcal{A}) \geq A_{val}(\mathcal{A}) - 2\epsilon$ and the test $|p_{FA}^{test} - p_{FA}| \leq \epsilon$, where $\epsilon = \sqrt{\frac{\log(|\mathcal{T}_1|) + \log(|\mathcal{T}_2|)}{\min(n_{neg}, n_{pos})}}$.*

The proof is in Appendix A. Note that this theorem implies we need to have $n_{neg}, n_{pos} = \Omega(\log(|\mathcal{T}_1|) + \log(|\mathcal{T}_2|))$ to guarantee the test AUROC is close to the convex-hull-AUROC on validation data. Furthermore, in Section 6, we validate through experiments that the selected thresholds transfer well to the test data.

6. Experiments

Datasets. We consider datasets widely used in research on hallucination detection (Kuhn et al., 2023; Farquhar et al., 2024; Lin et al., 2023; Nikitin et al., 2024). These datasets focus on reading comprehension and question-answering tasks, including TriviaQA (Joshi et al., 2017) for trivia knowledge, SQuAD (Rajpurkar et al., 2016) for general knowledge, and

Table 1: The minimum p (percentage of verifier calls) required to achieve $\alpha\%$ of the maximal AUROC gain (denoted as $p(\alpha)$) when Llama-3-70B-Instruct is the verifier, for different values of α . We report the average results across all target models on SQuAD (S), TriviaQA (T) and Natural Questions (N). The last column shows the maximal AUROC gain (Δ_{\max}).

	$p(70)$	$p(80)$	$p(90)$	$p(95)$	Δ_{\max}
S	$48.5_{\pm 7}$	$62.5_{\pm 11}$	$83.0_{\pm 5}$	$86.5_{\pm 5}$	$0.1_{\pm 0.03}$
T	$43.0_{\pm 3}$	$53.0_{\pm 2}$	$70.5_{\pm 8}$	$78.5_{\pm 10}$	$0.1_{\pm 0.02}$
N	$39.5_{\pm 6}$	$52.0_{\pm 10}$	$65.0_{\pm 6}$	$72.0_{\pm 6}$	$0.07_{\pm 0.00}$

Natural Questions (Kwiatkowski et al., 2019), derived from real user queries to Google Search.

Models. We consider: Llama-3-70B-Instruct, Llama-2-70b-chat-hf, Llama-2-13b-chat, Mixtral-8x7B-Instruct-v0.1 and merlinite-7b, which results in 20 target-verifier combinations. Following prior works (Lin et al., 2023; Kuhn et al., 2023; Nikitin et al., 2024), we use deberta-v2-xlarge-mnli as the entailment estimator and take the post-softmax probability corresponding to the ‘Entailment’ label as the output (ranging from 0 to 1).

Evaluation. We set $\tau = 0.1, \tau' = 1.0, m = 10$. To obtain the ground truth annotations for hallucination, we use GPT-4 as the judge. Performance is measured in terms of AUROC and AURAC as described in Section 6. Since this requires a validation set, we compare two scenarios: (1) the validation set consists of the same questions as the test set but with independently sampled random answers, and (2) the validation set consists of different questions from the same dataset. In both scenarios, the sizes of the validation and test sets are 400. First scenario represents an oracle setting, as the thresholds rely on the ground truth for the same questions. The second scenario reflects a practical setting where a separate set of questions is used to determine thresholds. We repeat the test with 5 random seeds and report the average result along with the standard deviation.

Estimation of computational overhead. Given that Alg. 1 focuses on budget awareness, it is important to consider both performance and budget in our evaluation. To quantify the additional computational cost introduced in Alg. 1 compared to the case where only self-consistency is used, we define a metric called *relative additional cost*:

$$\frac{\text{FLOPs(Alg. 1)} - \text{FLOPs(only self-consistency checking)}}{\text{FLOPs(only self-consistency checking)}},$$

which can be estimated as $\frac{pN_v}{N_t}$ using the FLOP estimation formula from (Kaplan et al., 2020) (detailed derivation Appx C.1). Here, N_t and N_v represent the number of non-embedding parameters in the target and verifier models, respectively. p accounts for the fact that the verifier model is queried for only a fraction p of the questions in Alg. 1.

Performance vs. cost. In Figs. 6 (AUROC) and 9 (AURAC) (in the supplement), we plot the detection performance against the estimated *relative additional cost* when varying p . A general trend observed is that when the verifier model is stronger than the target model (e.g., when the target is merlinite-7b and the verifier is Llama-3-70B-Instruct), increasing the computational budget—by allowing more verifier calls controlled by a larger p —monotonically improves performance. However, with a weaker verifier (e.g., when the target is Llama-3-70B-Instruct and the verifier is Llama-2-13b-chat), we observe an increasing-decreasing trend, where an intermediate number of verifier calls achieves the best results. This aligns with the intuition from Fig. 4, where intermediate weights on self-consistency cross-model-consistency are optimal, indicating that even a weaker verifier can contribute meaningfully to detection when an appropriate balance is maintained.

Our approach can achieve high performance with very low computational cost. The curves in Fig. 6 are convex, indicating that a small number of cross-model consistency checks contributing to most of the improvement in performance. To further illustrate this, we examine the minimum p required to achieve different percentages of performance gains when using Llama-3-70B-Instruct as the verifier in Table 1. Notably, compared to querying the verifier for all questions, we can reduce the cost by 13.5%–28% while retaining 95% of the gain (Δ_{\max}) in performance.

Selection of the verifier. Llama-3-70B-Instruct (blue), consistently achieves the best results when the computational budget is large. However, Mixtral-8x7B-Instruct-v0.1 (purple), stands out for its exceptional performance with a very small cost. This efficiency can be attributed to its MoE based design—despite having 46.7B total parameters, it only uses 12.9B parameters per token.

Transferability of thresholds. The gap between the scenarios where the validation set contains the same questions or different questions is overall small (dashed vs. solid lines, Fig 6), suggesting that the selection of thresholds transfers well to different questions, making the approach practical.

Comparison with approximated ceiling performance. The gap between our approach and the ceiling performance approximate using supervised learning with GCNs (described in Sec. 4.2.1; horizontal dashed line, Fig 6) is generally small. This indicates that our method effectively utilizes the verifier’s information despite not always querying it.

7. Conclusion

In this paper, we empirically analyzed consistency-based methods for hallucination detection. Based on this analysis, we introduced a budget-aware two-stage approach that leverages both self-consistency and cross-model consistency with a given verifier. Our method reduces computational cost by selectively querying the verifier. Extensive experiments demonstrate that it achieves strong performance with minimal computation, notably reducing computation by up to 28% while retaining 95% of the maximal performance gain.

Acknowledgement

This research was partially supported by the National Science Foundation CAREER Award 2146492.

References

- Agrawal, A., Suzgun, M., Mackey, L., and Kalai, A. T. Do language models know when they’re hallucinating references? *arXiv preprint arXiv:2305.18248*, 2023.
- Asai, A., Wu, Z., Wang, Y., Sil, A., and Hajishirzi, H. Self-rag: Learning to retrieve, generate, and critique through self-reflection. *arXiv preprint arXiv:2310.11511*, 2023.
- Duan, J., Cheng, H., Wang, S., Zavalny, A., Wang, C., Xu, R., Kailkhura, B., and Xu, K. Shifting attention to relevance: Towards the predictive uncertainty quantification of free-form large language models. In *Proceedings of the 62nd Annual Meeting of the Association for Computational Linguistics (Volume 1: Long Papers)*, pp. 5050–5063, 2024.
- Farquhar, S., Kossen, J., Kuhn, L., and Gal, Y. Detecting hallucinations in large language models using semantic entropy. *Nature*, 630(8017):625–630, 2024.
- Gao, L., Dai, Z., Pasupat, P., Chen, A., Chaganty, A. T., Fan, Y., Zhao, V. Y., Lao, N., Lee, H., Juan, D.-C., et al. Rarr: Researching and revising what language models say, using language models. *arXiv preprint arXiv:2210.08726*, 2022.
- Joshi, M., Choi, E., Weld, D., and Zettlemoyer, L. triviaqa: A Large Scale Distantly Supervised Challenge Dataset for Reading Comprehension. *arXiv e-prints*, art. arXiv:1705.03551, 2017.
- Kadavath, S., Conerly, T., Askell, A., Henighan, T., Drain, D., Perez, E., Schiefer, N., Hatfield-Dodds, Z., DasSarma, N., Tran-Johnson, E., et al. Language models (mostly) know what they know. *arXiv preprint arXiv:2207.05221*, 2022.
- Kalai, A. T. and Vempala, S. S. Calibrated language models must hallucinate. *Proceedings of the 56th Annual ACM Symposium on Theory of Computing (STOC)*, 2024. URL <https://arxiv.org/abs/2311.14648>.
- Kaplan, J., McCandlish, S., Henighan, T., Brown, T. B., Chess, B., Child, R., Gray, S., Radford, A., Wu, J., and Amodei, D. Scaling laws for neural language models. *arXiv preprint arXiv:2001.08361*, 2020.
- Kuhn, L., Gal, Y., and Farquhar, S. Semantic uncertainty: Linguistic invariances for uncertainty estimation in natural language generation. *arXiv preprint arXiv:2302.09664*, 2023.
- Kwiatkowski, T., Palomaki, J., Redfield, O., Collins, M., Parikh, A., Alberti, C., Epstein, D., Polosukhin, I., Kelcey, M., Devlin, J., Lee, K., Toutanova, K. N., Jones, L., Chang, M.-W., Dai, A., Uszkoreit, J., Le, Q., and Petrov, S. Natural questions: a benchmark for question answering research. *Transactions of the Association of Computational Linguistics*, 2019.

- Lee, N., Ping, W., Xu, P., Patwary, M., Fung, P. N., Shoeybi, M., and Catanzaro, B. Factuality enhanced language models for open-ended text generation. *Advances in Neural Information Processing Systems*, 35:34586–34599, 2022.
- Li, K., Patel, O., Viégas, F., Pfister, H., and Wattenberg, M. Inference-time intervention: Eliciting truthful answers from a language model. *Advances in Neural Information Processing Systems*, 36, 2024.
- Lin, S., Hilton, J., and Evans, O. Teaching models to express their uncertainty in words. *arXiv preprint arXiv:2205.14334*, 2022.
- Lin, Z., Trivedi, S., and Sun, J. Generating with confidence: Uncertainty quantification for black-box large language models. *arXiv preprint arXiv:2305.19187*, 2023.
- Manakul, P., Liusie, A., and Gales, M. J. Selfcheckgpt: Zero-resource black-box hallucination detection for generative large language models. *arXiv preprint arXiv:2303.08896*, 2023.
- Mielke, S. J., Szlam, A., Dinan, E., and Boureau, Y.-L. Reducing conversational agents’ overconfidence through linguistic calibration. *Transactions of the Association for Computational Linguistics*, 10:857–872, 2022.
- Muandet, K., Fukumizu, K., Sriperumbudur, B., and Schölkopf, B. Kernel mean embedding of distributions: A review and beyond. *Foundations and Trends® in Machine Learning*, 10(1–2):1–141, 2017. ISSN 1935-8245. doi: 10.1561/22000000060. URL <http://dx.doi.org/10.1561/22000000060>.
- Nikitin, A., Kossen, J., Gal, Y., and Martinen, P. Kernel language entropy: Fine-grained uncertainty quantification for llms from semantic similarities. *arXiv preprint arXiv:2405.20003*, 2024.
- Rajpurkar, P., Zhang, J., Lopyrev, K., and Liang, P. SQuAD: 100,000+ questions for machine comprehension of text. In Su, J., Duh, K., and Carreras, X. (eds.), *Proceedings of the 2016 Conference on Empirical Methods in Natural Language Processing*, pp. 2383–2392, Austin, Texas, November 2016. Association for Computational Linguistics. doi: 10.18653/v1/D16-1264. URL <https://aclanthology.org/D16-1264>.
- Tian, K., Mitchell, E., Yao, H., Manning, C. D., and Finn, C. Fine-tuning language models for factuality. *arXiv preprint arXiv:2311.08401*, 2023a.
- Tian, K., Mitchell, E., Zhou, A., Sharma, A., Rafailov, R., Yao, H., Finn, C., and Manning, C. D. Just ask for calibration: Strategies for eliciting calibrated confidence scores from language models fine-tuned with human feedback. *arXiv preprint arXiv:2305.14975*, 2023b.
- Varshney, N., Yao, W., Zhang, H., Chen, J., and Yu, D. A stitch in time saves nine: Detecting and mitigating hallucinations of llms by validating low-confidence generation. *arXiv preprint arXiv:2307.03987*, 2023.
- Xiong, M., Hu, Z., Lu, X., Li, Y., Fu, J., He, J., and Hooi, B. Can llms express their uncertainty? an empirical evaluation of confidence elicitation in llms. *arXiv preprint arXiv:2306.13063*, 2023.
- Yin, F., Srinivasa, J., and Chang, K.-W. Characterizing truthfulness in large language model generations with local intrinsic dimension. *arXiv preprint arXiv:2402.18048*, 2024.
- Zhang, J., Li, Z., Das, K., Malin, B., and Kumar, S. Sac3: Reliable hallucination detection in black-box language models via semantic-aware cross-check consistency. *arXiv preprint arXiv:2311.01740*, 2023. URL <https://arxiv.org/abs/2311.01740>.
- Zou, A., Phan, L., Chen, S., Campbell, J., Guo, P., Ren, R., Pan, A., Yin, X., Mazeika, M., Dombrowski, A.-K., et al. Representation engineering: A top-down approach to ai transparency. *arXiv preprint arXiv:2310.01405*, 2023.

A. Proof of Theorem 5.1

A classifier C maps points to binary predictions. The $p_D(C)$ is the probability that positive samples are mapped to 1, and $p_{FA}(C)$ is the probability that negative samples are mapped to 1. Hence

$$\hat{p}_D = \frac{1}{n_{neg}} \sum_i X_i^{neg}$$

$$\hat{p}_{FA} = \frac{1}{n_{pos}} \sum_i X_i^{pos}$$

where X_i^{neg} , X_i^{pos} are the labels of the positive and negative samples, respectively. These are each i.i.d. Bernoulli random variables.

The Hoeffding inequality can be directly applied:

$$Pr(|\hat{p}_D - p_D| \geq \epsilon) \leq 2 \exp(-2\epsilon^2 n_{neg})$$

and similarly for p_{FA} . Now, we want a uniform bound that holds simultaneously for all possible threshold combinations. The number of these are $|\mathcal{T}_1||\mathcal{T}_2|$.

Define events $\mathcal{E}_{j,k}^D$ and $\mathcal{E}_{j,k}^{FA}$ to be the events that the estimated probabilities under the j th, k th threshold are within ϵ , i.e.

$$\mathcal{E}_{j,k}^D := |\hat{p}_D(t_j^1, t_k^2) - p_D(t_j^1, t_k^2)| \leq \epsilon$$

$$\mathcal{E}_{j,k}^{FA} := |\hat{p}_{FA}(t_j^1, t_k^2) - p_{FA}(t_j^1, t_k^2)| \leq \epsilon.$$

Let's use the union bound across the j, k , we don't need it across FA/D, since these are independent.

$$Pr\left(\bigcap_{j=1}^{|\mathcal{T}_1|} \bigcap_{k=1}^{|\mathcal{T}_2|} (\mathcal{E}_{j,k}^D \cap \mathcal{E}_{j,k}^{FA})\right) \geq (1 - 2|\mathcal{T}_1||\mathcal{T}_2| \exp(-2\epsilon^2 n_{neg})) (1 - 2|\mathcal{T}_1||\mathcal{T}_2| \exp(-2\epsilon^2 n_{pos}))$$

In other words,

$$\max_{j,k} \max(|\hat{p}_D(t_j^1, t_k^2) - p_D(t_j^1, t_k^2)|, |\hat{p}_{FA}(t_j^1, t_k^2) - p_{FA}(t_j^1, t_k^2)|) \leq \sqrt{\frac{\log(|\mathcal{T}_1|) + \log(|\mathcal{T}_2|)}{\min(n_{neg}, n_{pos})}},$$

with probability at least $\left(1 - \frac{2}{|\mathcal{T}_1||\mathcal{T}_2|}\right)^2$. Since this holds simultaneously for all threshold combinations, if we take the training-convex-hull area, the test AUC from using the frontier of that hull will be at most 2ϵ smaller.

B. Kernel Mean Embedding View of Consistency Methods for Hallucination Detection

In what follows, we suppose that we have also access to the ground truth $\pi^*(y|x)$ and observe $\frac{1}{n^*} \sum_{i=1}^{n^*} \delta_{y_i^*}, y_i^* \sim \pi^*(\cdot|x)$.

Proposition B.1. *The optimal weight λ for combining self and cross consistencies to approximate the consistency of the target with the ground truth satisfies:*

$$\min_{\lambda \in [0,1]} |\langle \mu_t, \lambda \mu_t + (1-\lambda) \mu_v \rangle - \langle \mu_t, \mu^* \rangle| \leq \min_{\lambda \in [0,1]} \sqrt{2(1 - \langle \mu_*, \lambda \mu_t + (1-\lambda) \mu_v \rangle)},$$

Hence it is enough to solve: $\max_{\lambda \in [0,1]} \langle \mu_*, \lambda \mu_t + (1-\lambda) \mu_v \rangle$. Using an entropic regularization of this objective

$$\max_{\omega_t, \omega_v \in [0,1], \omega_t + \omega_v = 1} \langle \mu_*, \omega_t \mu_t + \omega_v \mu_v \rangle - \epsilon \left(\sum_{j \in \{t,v\}} \omega_j (\log \omega_j - 1) \right),$$

we obtain $\lambda^* = \frac{\exp(\frac{\langle \mu_t, \mu^* \rangle}{\epsilon})}{\exp(\frac{\langle \mu_t, \mu^* \rangle}{\epsilon}) + \exp(\frac{\langle \mu_v, \mu^* \rangle}{\epsilon})}$.

$$\begin{aligned}
 |\langle \mu_t, \lambda \mu_t + (1 - \lambda) \mu_v \rangle - \langle \mu_t, \mu^* \rangle| &= |\langle \mu_t, \mu^* - (\lambda \mu_t + (1 - \lambda) \mu_v) \rangle| \\
 &\leq \|\mu_t\| \|\mu^* - (\lambda \mu_t + (1 - \lambda) \mu_v)\| \\
 &\leq \sqrt{2(1 - \langle \mu^*, \lambda \mu_t + (1 - \lambda) \mu_v \rangle)},
 \end{aligned}$$

last inequality follows from $\|\mu^*\| \leq 1$, $\|\mu_t\| \leq 1$, $\|\mu_v\| \leq 1$ and $\|\lambda \mu_t + (1 - \lambda) \mu_v\| \leq 1$ (since the kernel \mathcal{E} is bounded by 1).

Hence to minimize this inequality it is enough to solve for :

$$\max_{\lambda \in [0,1]} \langle \mu^*, \lambda \mu_t + (1 - \lambda) \mu_v \rangle$$

we can add to this an entropy regularizer

$$\max_{\omega_t, \omega_v \in [0,1], \omega_t + \omega_v = 1} \langle \mu^*, \omega_t \mu_t + \omega_v \mu_v \rangle - \varepsilon \left(\sum_{j \in \{t,v\}} \omega_j (\log \omega_j - 1) \right)$$

which gives us that: $\lambda = \omega_t = \frac{\exp(\frac{\langle \mu_t, \mu^* \rangle}{\varepsilon})}{\exp(\frac{\langle \mu_t, \mu^* \rangle}{\varepsilon}) + \exp(\frac{\langle \mu_v, \mu^* \rangle}{\varepsilon})}$ and $\omega_v = 1 - \lambda = \frac{\exp(\frac{\langle \mu_v, \mu^* \rangle}{\varepsilon})}{\exp(\frac{\langle \mu_t, \mu^* \rangle}{\varepsilon}) + \exp(\frac{\langle \mu_v, \mu^* \rangle}{\varepsilon})}$.

C. Experimental Details

C.1. Estimation of computation cost

To compute the budget, we use the estimation formula derived in (Kaplan et al., 2020), Table 1, which states that the number of FLOPs per token is approximately $2N$ for models with sufficiently large dimensions, where N represents the number of non-embedding parameters in the model. Then, for each question, the computation cost of cross-model consistency checking can be expressed as:

$$ml_q 2N_{verifier} + m^2 l_a 2N_{deberta}, \quad (2)$$

where l_q is the number of tokens in the question, and l_a is the number of tokens in each answer (assuming all m answers share the same length), $N_{verifier}$, $N_{deberta}$ are the number of parameters of the verifier model and the entailment estimator (i.e., `deberta-v2-xlarge-mnli`), respectively. This estimation remains challenging due to the variability in the lengths of questions and answers, which depend on each specific question and model. To simplify this, we consider the scaling limit, where—assuming no restrictions—the lengths of questions and answers scale to the respective context lengths of the models processing them (since tokens exceeding the context length are dropped). Notably, the context length of `deberta-v2-xlarge-mnli` is only 512, while the context lengths of verifier models range from 4,096 to 128,000. Using this, we compute the ratio of the second term to the first term in Equation 2, which is $m \frac{l_a}{l_q} \frac{N_{deberta}}{N_{verifier}}$, in the limit where both lengths reach their maximum. We find that this ratio is no greater than 0.087 in the largest case in our settings, indicating a negligible contribution of the second term in the limit. Thus, we omit the second term to simplify the estimated additional computation per question to $ml_q 2N_{verifier}$. Similarly, we can derive the estimation for the cost of self-consistency checking as $ml_q 2N_{target}$. Based on this simplification, the metric *additional relative cost* can be estimated as $\frac{pN_{verifier}}{N_{target}}$, where p accounts for the fact that the verifier model is queried for only a fraction p of the questions in Algorithm 1.

C.2. Additional Results

Figure 7 shows the comparison between the performance of existing methods and the approximated ceiling performance in terms of AURAC. We observe a pattern consistent with that in Figure 2.

Figure 8 shows the AURAC performance against λ when using a weighted average of self-consistency and cross-consistency-based metrics, $(1 - \lambda)\text{MPD}(\mathbf{P}^{\text{self}}) + \lambda\text{MPD}(\mathbf{P}^{\text{cross}})$.

Figure 9 shows the AUROC performance of the two-stage detection method under varying computational budgets.

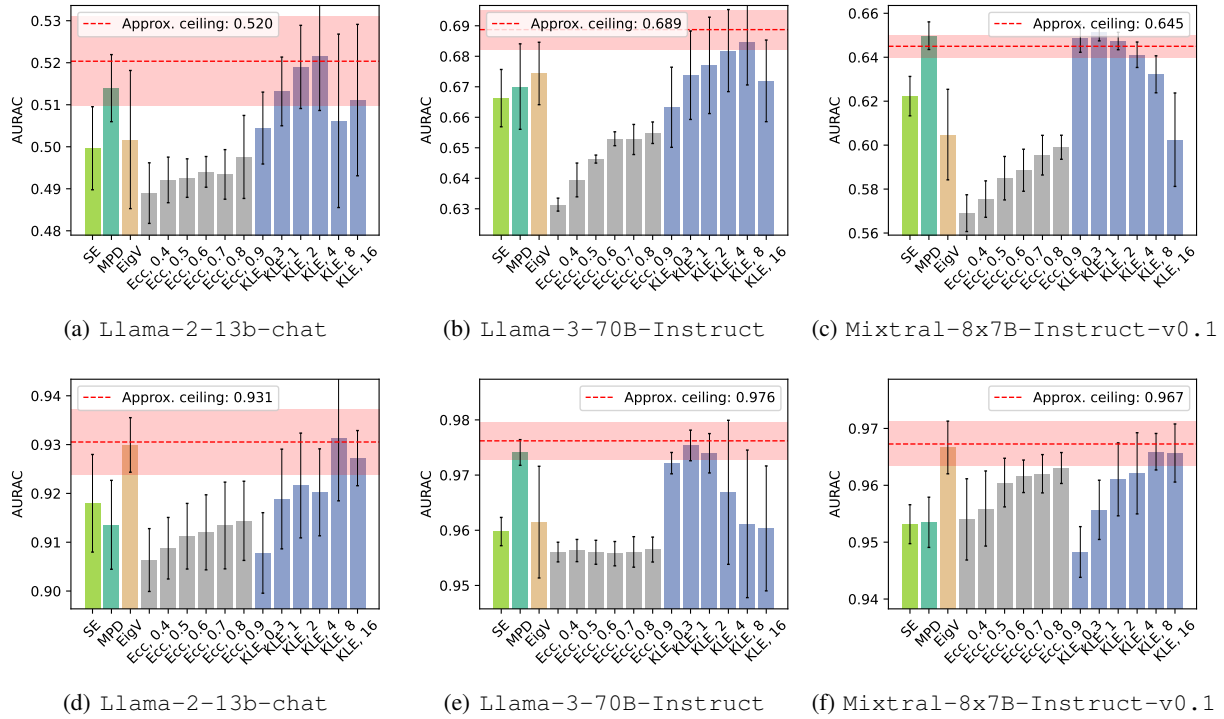


Figure 7: Comparison between the performance of existing methods and the approximated ceiling performance on the SQuAD ((a)–(c)) and TriviaQA ((d)–(f)) datasets. Here, performance is measured in terms of AURAC. We observe a pattern consistent with the discussion in Figure 2.

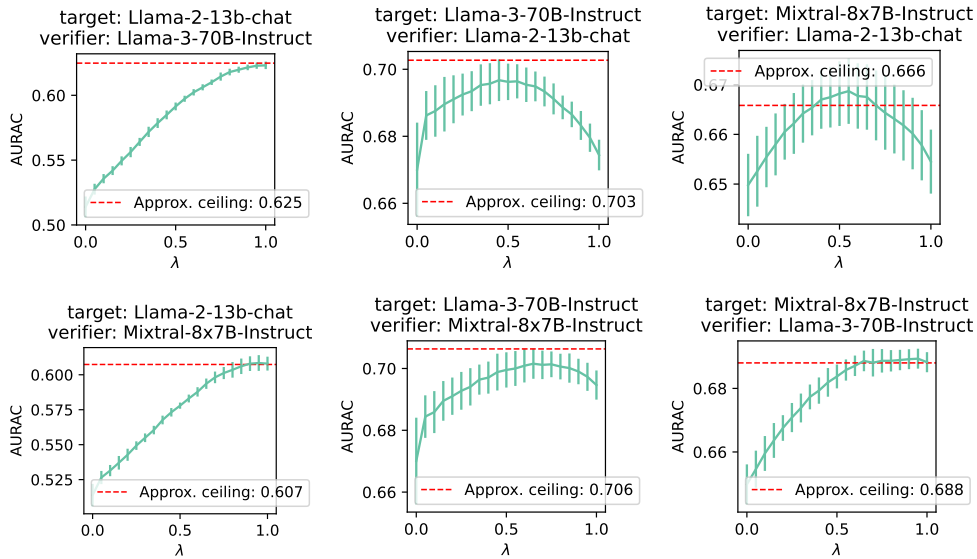


Figure 8: A simple weighted average of self-consistency and cross-consistency-based metrics, $(1 - \lambda)\text{MPD}(P^{\text{self}}) + \lambda\text{MPD}(P^{\text{cross}})$, can achieve performance close to that of the oracle method.

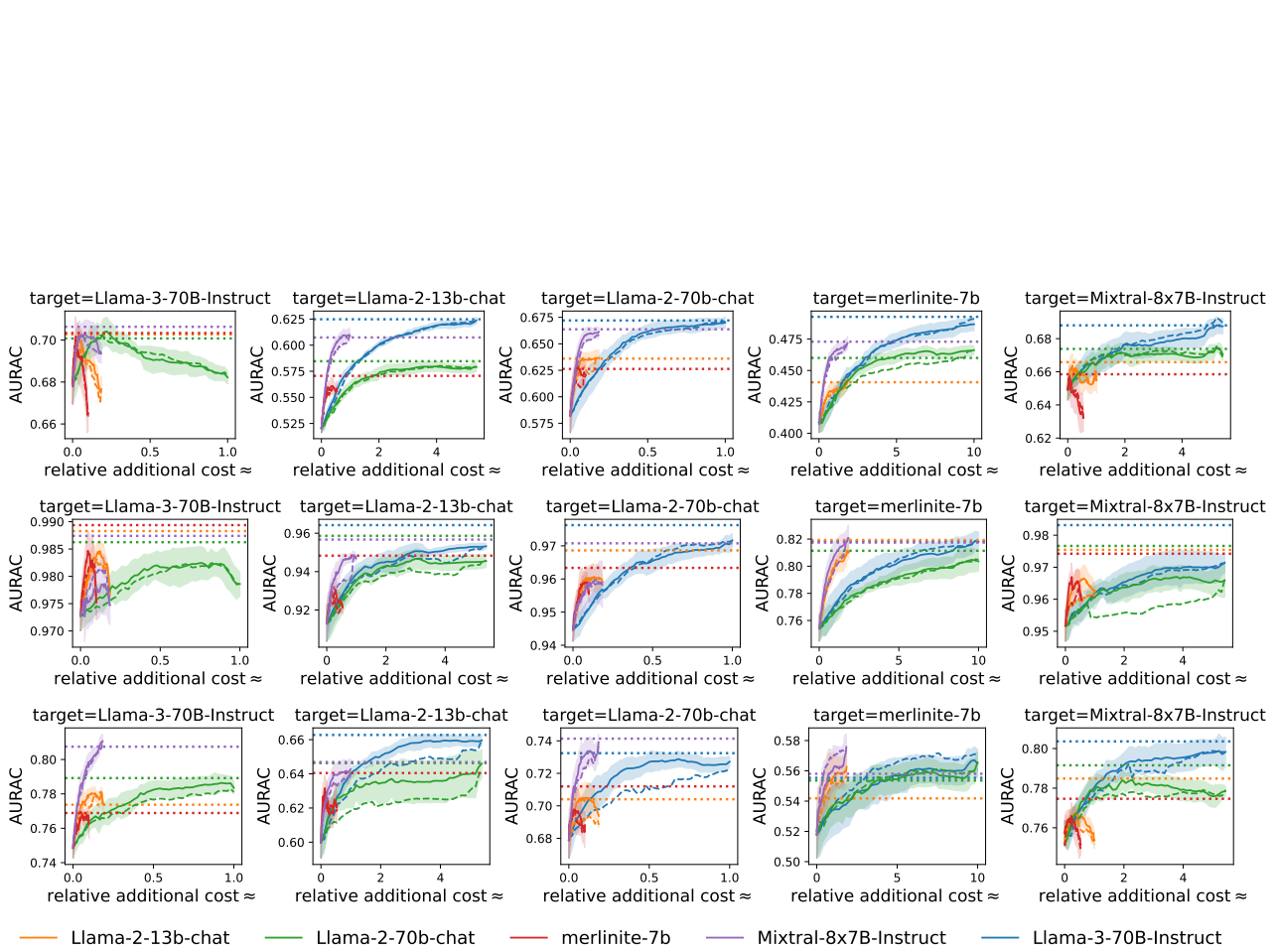


Figure 9: AURAC vs. relative additional cost for SQuAD (top), TriviaQA (middle), and Natural Questions (bottom).